Nano Res (2010) 3: 317–325
DOI 10.1007/s12274-010-1035-z
Research Article

One-Pot Synthesis and Strong Near-Infrared Upconversion Luminescence of Poly(acrylic acid)-Functionalized $YF_3:Yb^{3+}/Er^{3+}$ Nanocrystals

Leyu Wang[1] (✉), Yi Zhang[2], and Yanyu Zhu[2]

[1] State Key Laboratory of Chemical Resource Engineering, Beijing University of Chemical Technology, Beijing 100029, China
[2] College of Chemistry and Materials Science, Anhui Key Laboratory of Chemo-Biosensing, Anhui Normal University, Wuhu 241000, China

Received: 24 January 2010 / Revised: 2 March 2010 / Accepted: 3 March 2010

ABSTRACT

This paper describes the synthesis of new upconverting luminescent nanoparticles that consist of $YF_3:Yb^{3+}/Er^{3+}$ functionalized with poly(acrylic acid) (PAA). Unlike the upconverting nanocrystals previously reported in the literature that emit visible (blue–green–red) upconversion fluorescence, these as-prepared nanoparticles emit strong near-infrared (NIR, 831 nm) upconversion luminescence under 980 nm excitation. Scanning electron microscopy, transmission electron microscopy, and powder X-ray diffraction were used to characterize the size and composition of the luminescent nanocrystals. Their average diameter was about 50 nm. The presence of the PAA coating was confirmed by infrared spectroscopy. The particles are highly dispersible in aqueous solution due to the presence of carboxylate groups in the PAA coating. By carrying out the synthesis in the absence of PAA, $YF_3:Yb^{3+}/Er^{3+}$ nanorice materials were obtained. These nanorice particles are larger (~700 nm in length) than the PAA-functionalized nanoparticles and show strong typical visible red (668 nm), rather than NIR (831 nm), upconversion fluorescence. The new PAA-coated luminescent nanoparticles have the pottential be used in a variety of bioanalytical and medical assays involving luminescence detection and fluorescence imaging, especially *in vivo* fluorescence imaging, due to the deep penetration of NIR radiation.

KEYWORDS

YF_3 nanocrystals, NIR upconverting luminescence, poly(acrylic acid)

1. Introduction

During the past decades, magnetic nanoparticles [1, 2], noble metal nanocrystals [3], quantum dots (QDs) [4–7], and other kinds of luminescent nanomaterials [8–10] have been successfully prepared and widely used in the biological and medical fields. Due to their novel optical properties, QDs are preferable to organic dyes for biotagging applications. However, their poor biocompatibility and toxic constituents make it a considerable challenge to develop applications of these materials in *in vivo* imaging [11–13]. Furthermore, the ultraviolet–visible [14] excitation used for QDs and organic dyes will cause damage to biological samples as well as strong autofluorescence, and thus further affect the detection sensitivity when used for *in vivo* imaging [15–18]. Photon upconversion is an alternative process for the generation of visible

Address correspondence to lywang@mail.buct.edu.cn

emission (blue–green–red) by near-infrared (NIR) excitation. It is based on sequential photon absorption and energy transfer steps involving real metastable excited states of the chromophore [8, 18–22]. The unique luminescence properties of lanthanide ions incorporated in fluoride matrices have long been recognized and attracted great attention. Recent studies suggest that lanthanide fluorides, including YF_3, LaF_3, $NaLaF_4$, $NaGaF_4$, and $NaYF_4$ nanocrystals are useful upconversion matrices [8, 16, 19, 20, 23, 24]. After doping with Yb^{3+}/Er^{3+} or Yb^{3+}/Tm^{3+} ion-pairs, the resulting nanocrystals possess novel visible upconversion fluorescence. Their unique upconversion luminescence, especially their novel NIR emission [25, 26], makes these upconversion nanocrystals ideal as biolabels.

In order to increase the optical efficiency of doped nanocrystals, a shell of pure host material has been grown around the core particles to separate the light-emitting ions (Er^{3+} or Tm^{3+}) from solvent molecules and ligands on the nanoparticle surface [27, 28]. Although the existence of high vibrational frequencies resulting from organic surfactants coated on the particle surface will decrease the upconversion emission efficiency, this can sometimes be used to tune the upconversion emission color (green-to-red ratio) [27]. This paper describes a novel strategy to obtain the strong NIR (831 nm) upconversion emission of Er^{3+} ions, which has seldom been reported [25]. By using different kinds of surfactants, we obtained Yb^{3+}/Er^{3+} doped YF_3 nanocrystals with different sizes and upconversion emission colors. The YF_3:Yb^{3+}/Er^{3+}@PAA nanocrystals obtained using a coating of poly (acrylic acid) (PAA) are of particular interest, as they combine the advantage of strong NIR emission (831 nm) under NIR (980 nm) excitation with the advantage of high solubility in aqueous solution associated with the PAA coating. Their novel properties make them complementary to semiconductors and organic dyes currently used in biological and biomedical fields.

Biological tissue strongly absorbs UV radiation and shows strong background fluorescence under UV excitation. NIR radiation, however, shows excellent penetration in *in vivo* applications and causes no autofluorescence [16–18]. For highly efficient *in vivo* biolabeling, not only low autofluorescence but also deep optical excitation/emission penetration is very important. So, employing NIR (980 nm) radiation for photon upconversion excitation is preferable for *in vivo* imaging applications. However, most of the reported upconversion nanocrystals show visible emission, mainly from blue (470 nm), green (551 nm) to red (660 nm) [16–18], and there are few reported materials which emit NIR fluorescence such as 831 nm light [25]. For materials which emit strong visible fluorescence under 980 nm excitation, the visible emission is not easy to detect when the particle label is attached to tissues deep inside the animal, which limits their *in vivo* applications, especially for deep *in vivo* imaging. In our case, the as-prepared nanocrystals are especially suitable for *in vivo* imaging due to the deep penetration of NIR emission (831 nm) and excitation (980 nm). Furthermore, the materials are biocompatible due to the coating of PAA, as well as nontoxic, in contrast to selenium-containing QDs.

2. Experimental

2.1 Chemicals

All chemicals were analytical grade and used directly without further purification. $Y(NO_3)_3{\cdot}6H_2O$, $Yb(NO_3)_3{\cdot}6H_2O$, $Er(NO_3)_3{\cdot}6H_2O$, NaF, absolute ethanol, and ethylene glycol were obtained from Beijing Ouhe Chemical Reagents Company. Poly(acrylic acid) (PAA, M_w = 1800, Aldrich), polyethylene glycol (PEG, M_w = 8000, Sigma), and sodium dodecyl sulphonate (SDS, Beijing Chemical Reagents Company) were used as surfactants for the nanoparticle preparation. Deionized water was used throughout.

2.2 Synthesis of PAA-functionalized YF_3:Yb^{3+}/Er^{3+} nanocrystals

For bioapplications, a primary requirement is to obtain stable, aqueous colloidal dispersions of nanocrystals. This was achieved by a facile one-pot solvothermal method. Luminescent YF_3:Yb^{3+}/Er^{3+}@PAA nanocrystals were prepared using lanthanide nitrate salts and sodium fluoride as precursors in a mixture of ethylene glycol and ethanol with PAA as the surfactant. In brief, aqueous solutions of $Y(NO_3)_3{\cdot}6H_2O$ (2.125 mL, 0.4 mol/L), $Yb(NO_3)_3{\cdot}6H_2O$ (200 μL, 0.5 mol/L), and $Er(NO_3)_3{\cdot}6H_2O$ (100 μL, 0.05 mol/L) were added

to a mixture of ethanol (20 mL) and ethylene glycol (10 mL) under magnetic stirring. The sodium fluoride solution (3 mL, 1.0 mol/L) was then added, and the solution was thoroughly stirred for about 30 min. PAA (0.1 g) was added to the white colloidal solution and the stirring was maintained for another 30 min. The milky colloidal solution was subsequently transferred into a 50-mL Teflon lined autoclave and heated at 185 ˚C for 24 h. Finally, the reaction system was allowed to cool to room temperature. The composition of the resulting nanocrystals is $Y_{0.85}F_3$:$Yb_{0.1}^{3+}$/$Er_{0.05}^{3+}$@PAA. The final product was collected by means of centrifugation, washed twice with ethanol, and a third time with deionized water to remove any remaining reactants. The final white product was dispersed in deionized water by ultrasonciation and stored for later use. For X-ray diffraction (XRD) and Fourier transform infrared (FTIR) measurements, the white powder was dried at 100 ˚C overnight. In a control experiment, we obtained a nanorice material in the absence of PAA by using the same protocol as above.

2.3 Characterization

Transmission electron microscopy (TEM) images were obtained by using a JEOL JEM-1200EX transmission electron microscope with an accelerating voltage of 100 kV. A small drop of YF_3:Yb^{3+}/Er^{3+}@PAA nanocrystal solution was put on a carbon-coated copper grid. Scanning electron microscopy (SEM) images [29] were obtained using a field-emission scanning electron microscope (Hitachi, S-4800). An X-ray powder diffractometer (Shimadzu, XRD-6000) with Cu Kα radiation (λ = 1.540 60 Å) was used to record the XRD patterns of the samples. FTIR spectra were obtained using KBr pellets and a Nicolet-560 spectrophotometer. The fluorescence emission spectra were obtained on a Hitachi F-4500 fluorescence spectrophotometer with a 980 nm laser diode as the excitation source.

3. Result and discussion

3.1 SEM and TEM images of the as-prepared nanocrystals

Figure 1 shows SEM images of the YF_3:Yb^{3+}/Er^{3+}@PAA nanocrystals (a) and the YF_3:Yb^{3+}/Er^{3+} nanorice (b). The YF_3:Yb^{3+}/Er^{3+}@PAA nanocrystals (Fig. 1(a)) have a high degree of uniformity with a narrow dispersion

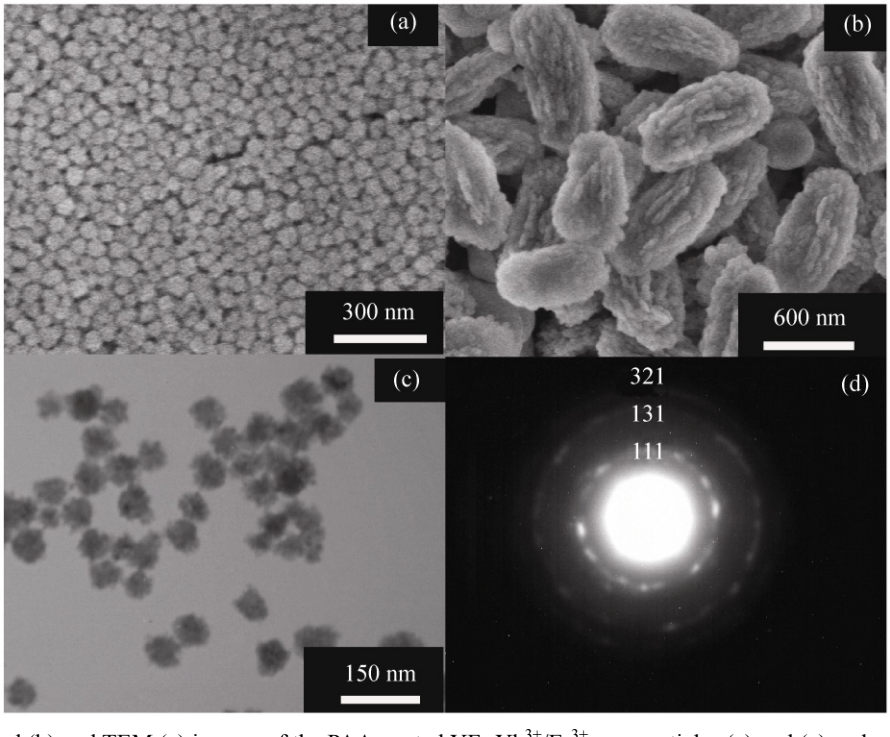

Figure 1 SEM (a) and (b) and TEM (c) images of the PAA-coated YF_3:Yb^{3+}/Er^{3+} nanoparticles (a) and (c) and uncoated YF_3:Yb^{3+}/Er^{3+} nanorice (b). (d) Electron diffraction pattern of the PAA-coated YF_3:Yb^{3+}/Er^{3+} nanoparticles shown in (c)

of particle size. Comparison of the image in Fig. 1(a) with that in Fig. 1(b) indicates that very different particles are produced by the same method of preparation in the presence (Fig. 1(a)) and absence (Fig. 1(b)) of PAA. In the absence of PAA as the surfactant, only large (~700 nm in length) nanorice particles were obtained instead of nanoparticles. The size difference is presumably caused by the strong chelating interaction between the lanthanide ions and the carboxylate groups in PAA. Due to this strong chelating effect, the lanthanide ions do not readily react with fluoride anions. After crystal seeds were formed in the initial reaction phase, PAA became coated onto the outer surface of the nanoparticles and consequently prevented the nanocrystals from growing to a large size. As a result, only small nanoparticles were obtained in the presence of PAA. However, in the absence of PAA, the particles had nothing coating their surface to limit their growth and finally grew to very large sizes. Figure 1(c) shows a TEM image of the sample prepared in the presence of PAA. The TEM image confirms the uniform shape and narrow size dispersion of the particles, with an average size of about 50 nm. The TEM image suggests that PAA is uniformly packed on the surface of YF_3:Yb^{3+}/Er^{3+} nanocrystals resulting in their uniform shape. From the SEM and TEM images, it is clear that both the nanoparticles and the nanorice particles are composed of small nanocrystals. The difference is that the size of these nanocrystals is larger for the nanorice than for the PAA-coated nanoparticles, because the crystal seeds are not able to grow very large in the presence of PAA due to the strong chelating interaction between the carboxylate and lanthanide ions. Although the-PAA coated nanoparticles consist of small nanocrystals, the electron diffraction pattern (Fig. 1(d)) demonstrates their good crystallinity and is consistent with the expected pattern for cubic YF_3.

3.2 XRD characterization of the YF_3 nanocrystals

Both the nanorice and PAA-coated nanoparticles were also characterized by powder XRD. The XRD patterns of YF_3:Yb^{3+}/Er^{3+}@PAA nanoparticles and YF_3:Yb^{3+}/Er^{3+} nanorice are depicted in Fig. 2. The peak positions and relative intensities for both nanoparticles and nanorice are in good agreement with the literature values for the 111, 201, 131, 321, 322, 341, and 223 reflections of the cubic phase structure of YF_3 (JCPDS 74-0911) [19]. A large number of weaker peaks are also seen in the pattern of the nanorice which are not observed in the pattern of the YF_3:Yb^{3+}/Er^{3+}@PAA nanoparticles, consistent with the larger crystallite size of the former. The XRD patterns in Fig. 2 are therefore consistent with the electron diffraction pattern shown in Fig. 1(d), and confirm that the YF_3:Yb^{3+}/Er^{3+}@PAA nanoparticles have the cubic YF_3 structure. In addition to the aforementioned particle sizes of 50 and 700 nm estimated from TEM and SEM images, respectively, we also can calculate the particle size using the Scherrer formula based on the broadening of the XRD peaks. However, when the particle size is over 50 nm, such calculations are not very accurate. Therefore, we have only calculated the size of the PAA-coated nanoparticles via the Scherrer formula. The calculated size is about 43.5 nm, which is slightly less than that suggested by the TEM images, which is reasonable because the nanoparticles shown in the TEM images are composed of smaller crystals.

3.3 FTIR characterization of the as-prepared nanocrystals

Due to the presence of the carboxylate groups in the PAA coating on the nanoparticle surface, the YF_3:Yb^{3+}/Er^{3+}@PAA nanocrystals possess excellent dispersibility

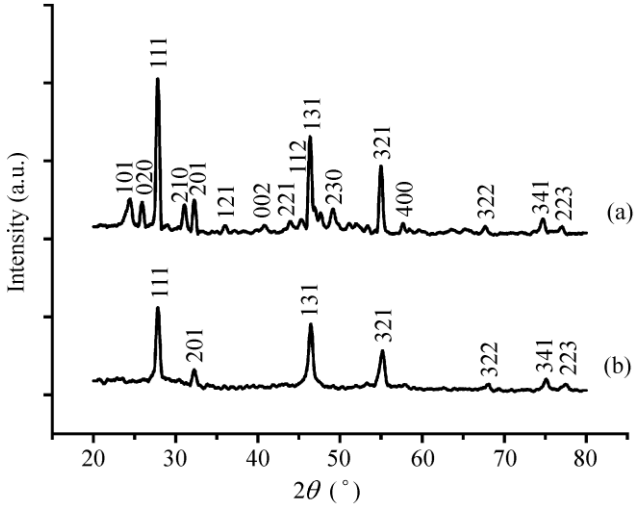

Figure 2 XRD patterns of YF_3:Yb^{3+}/Er^{3+} nanorice (a) and YF_3:Yb^{3+}/Er^{3+}@PAA nanoparticles (b)

in aqueous solution, as required for biological and biomedical applications. The PAA coating can be easily characterized by FTIR spectroscopy. Figure 3 shows the FTIR spectra of YF_3:Yb^{3+}/Er^{3+} nanorice and YF_3:Yb^{3+}/Er^{3+}@PAA nanoparticles. The absorption around 3441 cm^{-1} in the spectrum of the nanorice without a PAA coating (Fig. 3(a)) is assigned to O–H vibrations resulting from ethylene glycol or ethanol adsorbed on the YF_3 surface during the preparation process. The absorption peak around 1629 cm^{-1} can be attributed to the Y–O vibration in impurities caused by the presence of O_2 during the reaction. The strong peak at 468 cm^{-1} results from the Y–F vibrations. In the spectrum of YF_3:Yb^{3+}/Er^{3+}@PAA nanoparticles (Fig. 3(b)), the broad and strong stretching vibration band centered at 3491 cm^{-1} is characteristic of O–H in a –COOH group, and the peak at 2952 cm^{-1} is attributed to the methylene (CH_2) stretching vibrations of the long alkyl chain of PAA. The band at 1728 cm^{-1} is assigned to the C=O stretching vibration of the –COOH group, and the bands at 1571 and 1461 cm^{-1} result from the asymmetric and symmetric stretching vibrations, respectively, of the carboxylate group ($–COO^-$) in the PAA coating. The peak at 1422 cm^{-1} is due to the C–O stretching vibration in the –COOH groups of PAA. The significant differences between the spectra in Figs. 3(a) and 3(b) confirm that the nanocrystals have been surface-modified by PAA in the latter case.

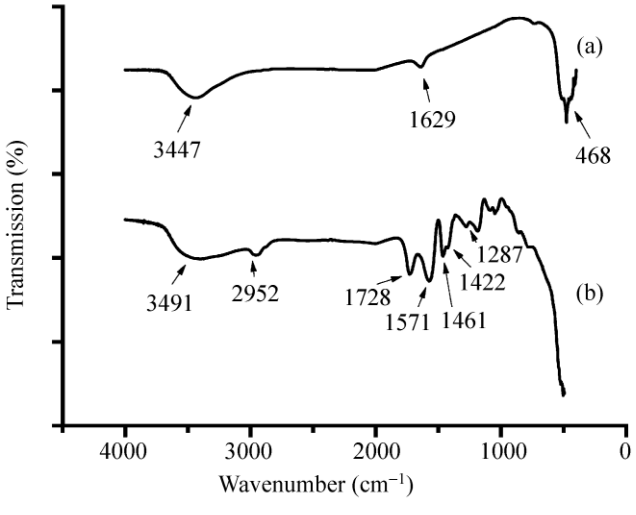

Figure 3 FTIR spectra of the YF_3:Yb^{3+}/Er^{3+} nanorice without PAA coating (a) and YF_3:Yb^{3+}/Er^{3+}@PAA nanoparticles (b)

3.4 Upconversion luminescence spectra of YF_3:Yb^{3+}/Er^{3+} nanorice and YF_3:Yb^{3+}/Er^{3+}@PAA nanoparticles

The novel upconversion luminescence for both YF_3:Yb^{3+}/Er^{3+} nanorice and YF_3:Yb^{3+}/Er^{3+}@PAA nanoparticles is demonstrated in Fig. 4. The emission peaks of YF_3:Yb^{3+}/Er^{3+} nanorice (Fig. 4(b)) are located at 551 nm (Er^{3+}: $^4S_{3/2}\rightarrow{}^4I_{15/2}$), 668 nm ($Er^{3+}$: $^4F_{9/2}\rightarrow{}^4I_{15/2}$) [19], and 831 nm ($Er^{3+}$: $^4S_{3/2}\rightarrow{}^4I_{13/2}$) [25]. The main emission centered at 668 nm is so strong that a very strong red luminescence in YF_3:Yb^{3+}/Er^{3+} is visible to the naked eye when a colloidal solution of the nanorice is irradiated at 980 nm with a laser diode. Although the red emission of YF_3:Yb^{3+}/Er^{3+} nanorice is very strong, the NIR emission at 831 nm is rather weak. Unlike the YF_3:Yb^{3+}/Er^{3+} nanorice, the YF_3:Yb^{3+}/Er^{3+}@PAA nanoparticles (Fig. 4(a)) show very weak blue emission at 417 nm and 488 nm. As shown in Fig. 4(a), these peaks can be assigned to the Er^{3+}: $^2H_{9/2}\rightarrow{}^4I_{15/2}$ and Er^{3+}: $^4F_{7/2}\rightarrow{}^4I_{15/2}$ transitions, respectively. It should be noted that such relatively weak blue emissions at 417 and 488 nm have seldom been reported [30]. The expected green emission at 551 nm and red emission at 668 nm, however, are too weak to be seen in the fluorescence spectra. It should be noted that the NIR upconversion luminescence at 831 nm is relatively strong. To the best of our knowledge, this NIR emission has seldom been previously reported for the Er^{3+} ion in the literature.

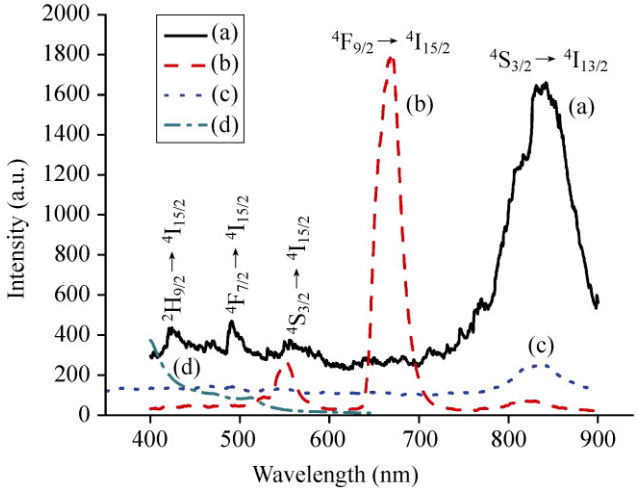

Figure 4 Upconversion luminescence spectra of (a) YF_3:Yb^{3+}/Er^{3+}@PAA nanoparticles, (b) YF_3:Yb^{3+}/Er^{3+} nanorice, and (c) YF_3:Er^{3+}@PAA nanoparticles under 980 nm laser excitation; (d) downconversion luminescence spectrum of YF_3:Er^{3+}@PAA nanoparticles under 345 nm excitation

3.5 Influence of Yb^{3+} ions on the upconversion luminescence of the nanocrystals

In order to investigate the luminescence under direct Er^{3+} excitation, we also prepared nanocrystals doped only with Er^{3+} using the same protocol employed for YF_3:Yb^{3+}/Er^{3+}@PAA nanoparticles. Not only the down-conversion but also the upconversion emission of the as-prepared YF_3:Er^{3+}@PAA nanoparticles was investigated. The visible emission spectrum under 345 nm excitation, depicted in Fig. 4(d), shows that no significant emission was observed. Figure 4(c) shows the NIR upconversion luminescence under 980 nm excitation and indicates that the emission intensity of YF_3:Er^{3+}@PAA nanoparticles is far weaker than that of YF_3:Yb^{3+}/Er^{3+}@PAA nanoparticles. We also prepared YF_3:Er^{3+} nanoparticles without Yb^{3+} codoping in the presence of other surfactants such as SDS and PEG. The upconversion emissions of these two kinds of nanoparticles were studied under 980 nm excitation. No NIR emission was observed around 831 nm, but a rather weak red fluorescence centered at 668 nm was observed (spectra not shown). These results indicate that the Yb^{3+} ion is a relatively efficient energy donor for the Yb^{3+}/Er^{3+} ion-pair NIR upconversion luminescence.

3.6 Influence of surfactants on the upconversion luminescence

In order to understand the mechanism responsible for the novel NIR emission observed above, we also prepared YF_3:Yb^{3+}/Er^{3+} nanoparticles with similar sizes by using different surfactants via the same protocol used for PAA. The sizes of all the nanoparticles coated with different kinds of surfactants are around 50 nm, and their SEM images are shown in Fig. S-1 in the Electronic Supplementary Material (ESM). Their upconversion emission spectra are depicted in Fig. 5. Although the particle sizes are similar, the luminescence properties are quite different. A very weak NIR (831 nm) upconversion emission is observed for the nanoparticles prepared at the presence of PEG. However, the red upconversion luminescence located at 668 nm is very strong in the case of this material. For the SDS-coated nanoparticles, emissions at both 668 nm and 831 nm are observed, and the intensity ratio $I_{831/668}$ is about 1.2. In contrast, the PAA-coated nanoparticles show rather strong NIR (831 nm) upconversion luminescence and no emission around 668 nm can be seen. These results indicate that the NIR emission is probably associated with novel surface properties rather than particle size.

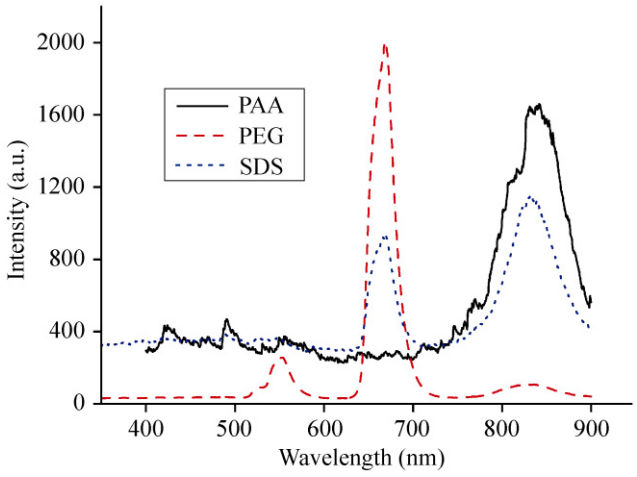

Figure 5 Upconversion luminescence spectra of YF_3:Yb^{3+}/Er^{3+} nanoparticles coated with PAA (solid line), PEG (dashed line), and SDS (dotted line). The average size of the nanoparticles coated with the different surfactants is around 50 nm in each case

3.7 Upconversion luminescence mechanism of the nanocrystals

In order to better understand the mechanism of upconversion emission, the upconversion excitation pathways for the Yb^{3+}/Er^{3+} ion-couple are depicted in Fig. 6. An initial energy transfer from a Yb^{3+} ion in the $^2F_{7/2}$ state to an Er^{3+} ion populates the $^4I_{15/2}$ level. Then another 980 nm photon, or energy transfer from a Yb^{3+} ion, can populate the $^4F_{7/2}$ level of the Er^{3+} ion. The Er^{3+} ions can then relax without emission to the $^2H_{11/2}$ and $^4S_{3/2}$ levels. The green emission bands at 551 nm and 525 nm can be attributed to the Er^{3+}: $^4S_{3/2}\rightarrow{}^4I_{15/2}$ and Er^{3+}: $^2H_{11/2}\rightarrow{}^4I_{15/2}$ transitions, respectively. Because of the short lifetime of the $^4I_{11/2}$ level, some ions in this level will decay nonradiatively to the long-lived $^4I_{13/2}$ level, and then be excited to the $^4F_{9/2}$ level via energy transfer from excited Yb^{3+} ions. Thus, the red emission at 668 nm can be obtained when the Er^{3+} ion at $^4F_{9/2}$ state relaxes to the ground state ($^4I_{15/2}$). The 831 nm emission can be obtained via multiphoton energy transfer, and shows relatively strong luminescence in the

near-infrared region. This emission results from the $^4S_{3/2}\rightarrow{}^4I_{13/2}$ transition [25]. The blue emissions centered at 417 nm and 488 nm can be assigned to Er^{3+}: $^2H_{9/2}\rightarrow{}^4I_{15/2}$ and Er^{3+}: $^4F_{7/2}\rightarrow{}^4I_{15/2}$ transitions, respectively [19, 30]. As shown in Fig. 4, the upconversion emission of YF_3@PAA nanoparticles doped with only Er^{3+} is far weaker than that of Yb^{3+}/Er^{3+} ion-pair doped YF_3@PAA nanoparticles. This indicates that the luminescence efficiency of direct Er^{3+} excitation is too low, confirming that the NIR emission is mainly due to the $Yb^{3+}\rightarrow Er^{3+}$ energy transfer process as depicted in Fig. 6.

In order to further understand the upconversion mechanism in these as-prepared nanoparticles, the intensities of the upconversion emissions were recorded as a function of the 980 nm excitation intensity. At low excitation power density, the output intensity (I_o) will be proportional to some power (n) of the infrared excitation (I_{IR}) power. The value of n is the number of IR photons absorbed per emission photon as shown in the following formula: $\ln I_o \propto n\cdot\ln I_{IR}$ [25]. As shown in Fig. 7, the slopes of the plots (n) are 1.92 and 2.11 for the green (551 nm) and red (668 nm) emissions, respectively. These double logarithmic plots of the visible upconversion emission intensity versus the power density of the 980 nm excitation confirm that both the 551 and 668 nm emissions involve two-photon upconversion processes. At high excitation densities the slope of the curves is reduced due to upconversion process saturation [31]. However, for the NIR (831 nm) emission of the PAA-coated nanoparticles, the slope of the plot is 2.71, which indicates that the upconversion emission is a three-photon process. Because of the strong chelating effect of PAA, the nanoparticle surface is coated with PAA molecules, as shown by TEM and FTIR spectroscopy. Due to the high vibrational frequency of –COOH and –OH groups in the PAA moieties coated on the nanoparticle surface, cross-relaxation is significant, and this might be responsible for the NIR emission [27]. More detailed research into the exact cause of the NIR emission is still underway.

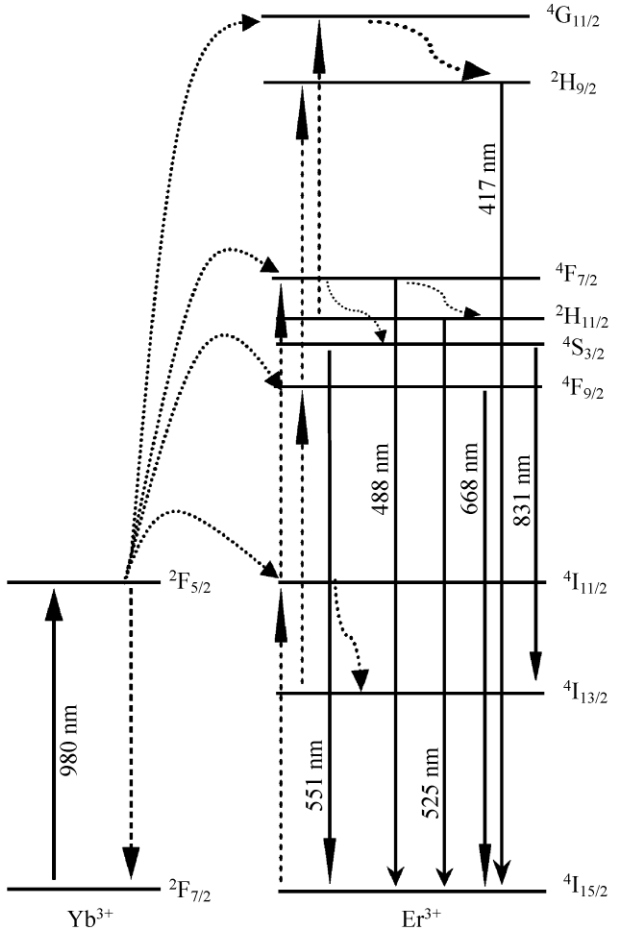

Figure 6 Scheme showing the mechanism of upconversion luminescence

4. Conclusions

We have successfully prepared luminescent YF_3:Yb^{3+}/Er^{3+} nanorice and YF_3:Yb^{3+}/Er^{3+}@PAA nanoparticles by using different surfactants. In the absence of PAA as a

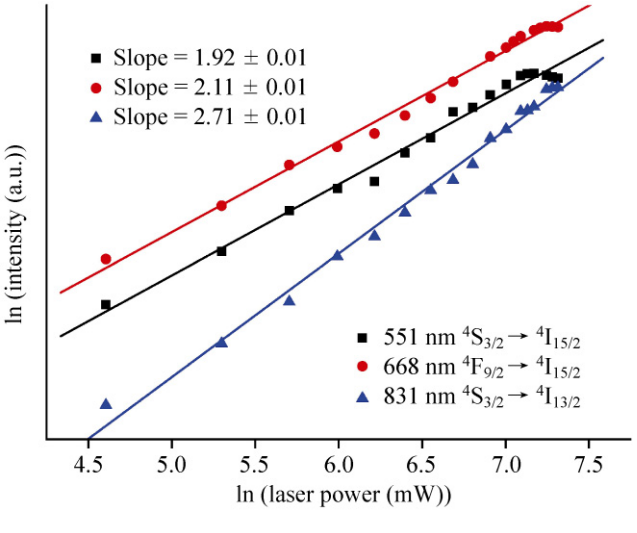

Figure 7 Power dependence of the upconversion luminescence of the YF_3:Yb^{3+}/Er^{3+}@PAA nanoparticles (▲) and YF_3:Yb^{3+}/Er^{3+} nanorice (● and ■) excited at 980 nm

surfactant, only large nanorice particles were obtained. These nanorice particles are very large (~700 nm in length) and show strong red upconversion fluorescence visible to the naked eye. However, in the presence of PAA as a surfactant, nanoparticles with a uniform size of ~50 nm, good dispersibility, and a large number of surface carboxylate groups were obtained. Unlike the nanorice materials, these luminescent nanoparticles emit strong NIR (831 nm) upconverting luminescence at 980 nm excitation. This novel NIR upconversion luminescence and the carboxylate-coated surface make these nanoparticles good candidates for biolabeling applications, especially for deep *in vivo* imaging due to the deep penetration of NIR radiation into tissue. Upconversion imaging studies are underway and will be reported elsewhere and suggest that these novel nanophosphors are promising candidates for applications as active components for fluorescence immunoassays, cell imaging, and especially as fluorescent labels for *in vivo* imaging with deep penetration.

Acknowledgements

We acknowledge the financial support from the National Natural Science Foundation of China (Nos. 20605001 and 20871004) and start-up funding of Beijing University of Chemical Technology.

Electronic Supplementary Material: SEM images of nanoparticles prepared using PAA, PEG and SDS as the surfactants are available in the online version of this article at http://dx.doi.org/10.1007/s12274-010-1035-z and are accessible free of charge.

References

[1] Ge, J. P.; Hu, Y. X.; Biasini, M.; Beyermann, W. P.; Yin, Y. D. Superparamagnetic magnetite colloidal nanocrystal clusters. *Angew. Chem. Int. Edit.* **2007**, *46*, 4342–4345.

[2] Wang, L. Y.; Yang, Z. H.; Zhang, Y.; Wang, L. Bifunctional nanoparticles with magnetization and luminescence. *J. Phys. Chem. C* **2009**, *113*, 3955–3959.

[3] Hill, H. D.; Hurst, S. J.; Mirkin, C. A. Curvature-induced base pair "slipping" effects in DNA-nanoparticle hybridization. *Nano Lett.* **2009**, *9*, 317–321.

[4] Bruchez, M.; Moronne, M.; Gin, P.; Weiss, S.; Alivisatos, A. P. Semiconductor nanocrystals as fluorescent biological labels. *Science* **1998**, *281*, 2013–2016.

[5] Chan, W. C. W.; Nie, S. M. Quantum dot bioconjugates for ultrasensitive nonisotopic detection. *Science* **1998**, *281*, 2016–2018.

[6] Gao, X. H.; Cui, Y. Y.; Levenson, R. M.; Chung, L. W. K.; Nie, S. M. *In vivo* cancer targeting and imaging with semiconductor quantum dots. *Nat. Biotechnol.* **2004**, *22*, 969–976.

[7] Viswanatha, R.; Battaglia, D. M.; Curtis, M. E.; Mishima, T. D.; Johnson, M. B.; Peng, X. Shape control of doped semiconductor nanocrystals (d-dots). *Nano Res.* **2008**, *1*, 138–144.

[8] Sivakumar, S.; Diamente, P. R.; van Veggel, F. C. Silica-coated Ln^{3+}-doped LaF_3 nanoparticles as robust down- and upconverting biolabels. *Chem. -Eur. J.* **2006**, *12*, 5878–5884.

[9] Santra, S.; Yang, H.; Dutta, D.; Stanley, J. T.; Holloway, P. H.; Tan, W. H.; Moudgil, B. M.; Mericle, R. A. TAT conjugated, FITC doped silica nanoparticles for bioimaging applications. *Chem. Commun.* **2004**, 2810–2811.

[10] Wang, L. Y.; Li, Y. D. Green upconversion nanocrystals for DNA detection. *Chem. Commun.* **2006**, 2557–2559.

[11] Yezhelyev, M. V.; Qi, L.; Regan, R. M. O.; Nie, S.; Gao, X. Proton-sponge coated quantum dots for siRNA delivery and intracellular imaging. *J. Am. Chem. Soc.* **2008**, *130*, 9006–9012.

[12] Mancini, M. C.; Kairdolf, B. A.; Smith, A. M.; Nie, S. Oxidative quenching and degradation of polymer-encapsulated quantum dots: New insights into the long-term fate and toxicity of nanocrystals *in vivo*. *J. Am. Chem. Soc.* **2008**, *130*, 10836–10837.

[13] King-Heiden, T. C.; Wiecinski, P. N.; Mangham, A. N.; Metz, K. M.; Nesbit, D.; Pedersen, J. A.; Hamers, R. J.; Heideman, W.; Peterson, R. E. Quantum dot nanotoxicity assessment using the zebrafish embryo. *Environ. Sci. Technol.* **2009**, *43*, 1605–1611.

[14] Gouveia-Neto, A. S.; da Costa, E. B.; Bueno, L. A; Ribeiro, S. J. L. Intense red upconversion emission in infrared excited holmium-doped $PbGeO_3$–PbF_2–CdF_2 transparent glass ceramic. *J. Lumin.* **2004**, *110*, 79–84.

[15] Wang, L. Y.; Li, Y. D. $Na(Y_{1.5}Na_{0.5})F_6$ single-crystal nanorods as multicolor luminescent materials. *Nano Lett.* **2006**, *6*, 1645–1649.

[16] Yi, G. S.; Lu, H. C.; Zhao, S. Y.; Yue, G.; Yang, W. J.; Chen, D. P.; Guo, L. H. Synthesis, characterization, and biological application of size-controlled nanocrystalline $NaYF_4$: Yb, Er infrared-to-visible up-conversion phosphors. *Nano Lett.* **2004**, *4*, 2191–2196.

[17] Wang, L. Y.; Yan, R. X.; Hao, Z. Y.; Wang, L.; Zeng, J. H.; Bao, J.; Wang, X.; Peng, Q.; Li, Y. D. Fluorescence resonant energy transfer biosensor based on upconversion-luminescent nanoparticles. *Angew. Chem. Int. Edit.* **2005**, 44, 6054–6057.

[18] van de Rijke, F.; Zijlmans, H.; Li, S.; Vail, T.; Raap, A. K.; Niedbala, R. S.; Tanke, H. J. Up-converting phosphor reporters for nucleic acid microarrays. *Nat. Biotechnol.* **2001**, *19*, 273–276.

[19] Yan, R. X.; Li, Y. D. Down/up conversion in Ln^{3+}-doped YF_3 nanocrystals. *Adv. Funct. Mater.* **2005**, *15*, 763–770.

[20] Heer, S.; Kompe, K.; Gudel, H. U.; Haase, M. Highly efficient multicolour upconversion emission in transparent colloids of lanthanide-doped $NaYF_4$ nanocrystals. *Adv. Mater.* **2004**, *16*, 2102–2104.

[21] Gao, L.; Ge, X.; Chai, Z.; Xu, G.; Wang, X.; Wang, C. Shape-controlled synthesis of octahedral α-$NaYF_4$ and its rare earth doped submicrometer particles in acetic acid. *Nano Res.* **2009**, *2*, 565–574.

[22] Yu, X.; Li, M.; Xie, M.; Chen, L.; Li, Y.; Wang, Q. Dopant-controlled synthesis of water-soluble hexagonal $NaYF_4$ nanorods with efficient upconversion fluorescence for multicolor bioimaging. *Nano Res.* **2010**, *3*, 51–60.

[23] Mai, H. X.; Zhang, Y. W.; Si, R.; Yan, Z. G.; Sun, L. D.; You, L. P.; Yan, C. H. High-quality sodium rare-earth fluoride nanocrystals: Controlled synthesis and optical properties. *J. Am. Chem. Soc.* **2006**, *128*, 6426–6436.

[24] Wang, L. Y.; Li, P.; Li, Y. D. Down- and up-conversion luminescent nanorods. *Adv. Mater.* **2007**, *19*, 3304–3307.

[25] Boyer, J. C.; Cuccia, L. A.; Capobianco, J. A. Synthesis of colloidal upconverting $NaYF_4$: Er^{3+}/Yb^{3+} and Tm^{3+}/Yb^{3+} monodisperse nanocrystals. *Nano Lett.* **2007**, *7*, 847–852.

[26] Boyer, J. C.; Vetrone, F.; Cuccia, L. A.; Capobianco, J. A. Synthesis of colloidal upconverting $NaYF_4$ nanocrystals doped with Er^{3+}, Yb^{3+} and Tm^{3+}, Yb^{3+} via thermal decomposition of lanthanide trifluoroacetate precursors. *J. Am. Chem. Soc.* **2006**, *128*, 7444–7445.

[27] Wang, Y.; Tu, L.; Zhao, J.; Sun, Y.; Kong, X.; Zhang, H. Upconversion luminescence of β-$NaYF_4$: Yb^{3+}, Er^{3+}@β-$NaYF_4$ core/shell nanoparticles: Excitation power density and surface dependence. *J. Phys. Chem. C* **2009**, *113*, 7164–7169.

[28] Schafer, H.; Ptacek, P.; Zerzouf, O.; Haase, M. Synthesis and optical properties of KYF_4/Yb, Er nanocrystals, and their surface modification with undoped KYF_4. *Adv. Funct. Mater.* **2008**, *18*, 2913–2918.

[29] Grogan, M. J.; Kaizuka, Y.; Conrad, R. M.; Groves, J. T.; Bertozzi, C. R. Synthesis of lipidated green fluorescent protein and its incorporation in supported lipid bilayers. *J. Am. Chem. Soc.* **2005**, *127*, 14383–14387.

[30] Capobianco, J. A.; Vetrone, F.; Boyer, J. C.; Speghini, A.; Bettinelli, M. Enhancement of red emission ($^4F_{9/2}$–$^4I_{15/2}$) via upconversion in bulk and nanocrystalline cubic Y_2O_3 : Er^{3+}. *J. Phys. Chem. B* **2002**, *106*, 1181–1187.

[31] Suyver, J. F.; Aebischer, A.; Garcia-Revilla, S.; Gerner, P.; Gudel, H. U. Anomalous power dependence of sensitized upconversion luminescence. *Phys. Rev. B* **2005**, *71*, 125123.